ISSN (Print) 1226-1750
ISSN (Online) 2233-6656
Journal of Magnetics 22(4), 642-648 (2017) https://doi.org/10.4283/JMAG.2017.22.4.642

Magnetic Field and Permeability Effects on Jeffrey Fluid in Eccentric Tubes Having Flexible Porous Boundaries

Arshad Riaz[1]*, Abdul Razaq[1], and Aziz Ullah Awan[2]

[1]*Department of Mathematics, University of Education Lahore, Jauharabad Campus 41200, Jauharabad, Pakistan*
[2]*Department of Mathematics, University of the Punjab Lahore, Pakistan*

(Received 23 September 2017, Received in final form 3 November 2017, Accepted 6 November 2017)

In the present study, we recapitulated the magnetic field and porous medium effects on the peristaltic mechanism of a Jeffrey fluid model observed between two electrically conducting eccentric annuli. The inner annulus is assumed to be rigid and to contain constant velocity across the longitudinal direction of the enclosure; the outer one is considered to be flexible and to experience peristaltic waves travelling down its walls. Moreover, the magnetic field is examined in the direction normal to the pattern in the presence of a porous medium. The flow, meanwhile, is incompressible and follows in an unsteady format. The flow's descriptive equations are reduced by anticipation of long wave length and small Reynolds number approximations. The resulting governing equations are then handled using analytical techniques. The achieved expressions for the considerable functions are manipulated graphically to determine the influences of various appertaining parameters. Finally, the results are compared with those of previous studies to confirm the validity of the present solutions through tables and graphs. The graphs indicated that the magnetic field increases the pumping rate but that the porosity reduces it.

Keywords : peristaltic transport, porous medium, eccentric cylinders, Jeffrey fluid, magnetohydrodynamics

1. Introduction

The peristaltic mechanism of fluids in three-dimensional geometries (tubes/ducts) has a special allure among to researchers. Peristalsis suggests a wave-like phenomenon that occurs due to involuntary expansion and contraction of a lissome wall. A large number of applications of peristaltic flow have been proved in different fields such as physiology, engineering and medicine. In many surgical processes for example, it is applied to circulate the blood in heart-lung machines. Naturally too, this process propagates to the intestines, stomach and esophagus. Many scientists and engineers have explored varieties of pumping machines very similar to roller pumps. The peristaltic mechanism of a toxic liquid is employed in the nuclear industry to retrieve penetration of the external environment [1]. The variable magnetic field acting on the peristaltic flow of Jeffrey fluid in a non-uniform rectangular duct having compliant walls has been investigated by Bhatti *et al.* [2]. Bhatti *et al*. [3] have examined the heat and mass transfer of two-phase flow with electric double-layer effects induced due to peristaltic propulsion in the presence of a transverse magnetic field. An extensive literature is available for analysis of the peristaltic transport of Newtonian and non-Newtonian fluids in various flow patterns [4-7]. Reddy *et al*. [8] have discussed the influence of lateral walls on the peristaltic flow in a rectangular duct. And, In order to simplify the problem, they have measured the results under the implementation of long wavelength and low Reynolds number. After a thorough review of the literature, it is found that only a few studies have analyzed the effect of the eccentricity attribute [9-11]. In recent years, the peristaltic flow of non-Newtonian fluids through eccentric cylinders has been investigated by some researchers. Recently, a mathematical model of peristaltic transport through eccentric cylinders was presented by Mekheimer *et al.* [12], who [13] have also executed the particulate suspension flow induced by sinusoidal peristaltic waves through eccentric cylinders with thread annular. Ellahi *et al.* [14] presented a series of solutions for the magnetohydrodynamic peristaltic flow of a Jeffrey fluid in eccentric cylinders.

*Corresponding author: Tel: 03006076036
Fax: 03455992002, e-mail: arshadriaz26@gmail.com

Keeping in mind the above discussion, the effects of a magnetic field and porous medium on the peristaltic flow of an electrically conducting non-Newtonian Jeffrey fluid has not yet been analyzed across eccentric cylinders. So, the motive of the present paper was to focus on the permeability of surrounding walls and MHD on Jeffrey fluid in the mid space of two eccentric annuli. An inspiration was the anticipation that this investigation would be beneficial to many industrial and engineering procedures. This idea, moreover, would provide a better solution for determination of the injection intensity and the fluid flow practice within the syringe. The governing equations for unsteady and incompressible flow of Jeffrey fluid are reduced by applying the assumptions of a long wave length. The simplified form of the equations is solved by using the series solution. The behavior of the flow for all of the respective parameters is investigated by means of graphs of the solutions and important flow features.

2. Mathematical Formulation of the Problem

Here, we examine the effects of a porous medium and MHD on the peristaltic mechanism of Jeffrey fluid in a three-dimensional rectangular channel. The sketch of the flow geometry is arranged such that the tube in the inside region is rigid with radius δ, and the outer tube experiences sinusoidal peristaltic waves aligned with its wall. It should be noted here that the fluid motion is observed to the centre of the upper cylinder (Fig. 1). Accordingly, the wall of the inner tube is represented by $r_1 = \delta + \varepsilon \cos\theta$, where the parameter ε represents the eccentricity of the inner tube. The walls are considered to be electrically conducting and passing in a rectangular channel across a porous medium.

The radii are suggested by the equations as [12]

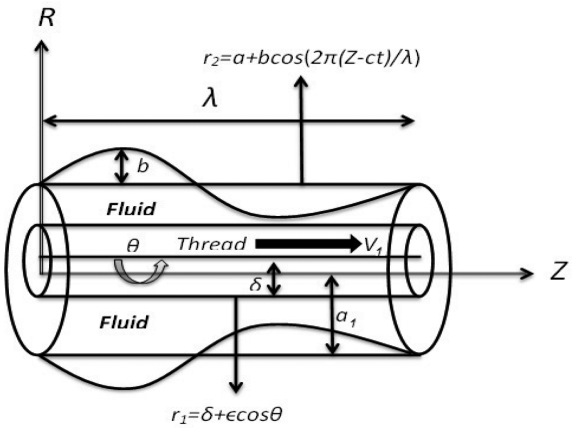

Fig. 1. Geometry of the problem.

$$r_1 = \delta + \varepsilon \cos\theta, \tag{1}$$

$$r_2 = a + b\cos\left[\frac{2\pi}{\lambda}(z - ct)\right], \tag{2}$$

where δ and a are the radii of the inner and outer tubes, b is the amplitude of the wave, and c is the velocity of wave's propagation. The laws of conservation and momentum for an incompressible non-Newtonian fluid with velocity vector (v, o, u) are presented as [12]

$$\frac{\partial u}{\partial z} + \frac{\partial v}{\partial r} + \frac{v}{r} = 0, \tag{3}$$

$$\rho\left[\frac{\partial v}{\partial t} + u\frac{\partial v}{\partial z} + v\frac{\partial v}{\partial r}\right] = -\frac{\partial p}{\partial r} + \frac{1}{r}\frac{\partial}{\partial r}(rS_{rr}) + \frac{1}{r}\frac{\partial}{\partial \theta}(S_{r\theta}) + \frac{\partial}{\partial z}(S_{rz}) - \frac{S_{\theta\theta}}{r} - \sigma B_0^2 v - \frac{\mu}{k_1}v, \tag{4}$$

$$0 = -\frac{1}{r}\frac{\partial p}{\partial \theta} + \frac{1}{r^2}\frac{\partial}{\partial r}(r^2 S_{r\theta}) + \frac{1}{r}\frac{\partial}{\partial \theta}(S_{\theta\theta}) + \frac{\partial}{\partial z}(S_{\theta z}), S \tag{5}$$

where v and u are the radial and normal velocity components, respectively, p stands for the pressure, μ is the viscosity, k_1 denotes the porous medium permeability, σ denotes the electric current density, B_0 is the magnetic field exerted normal to the direction of the flow, S indicates the stress tensor that is given in the subsequent form [5]

$$\mathbf{S} = \frac{\mu}{1 + \lambda_1}(\dot{\gamma} + \lambda_2 \ddot{\gamma}), \tag{6}$$

where λ_1 is the ratio of relaxation to retardation time, λ_2 is the delay time, $\dot{\gamma}$ is the shear rate, and the dots represent the derivatives with time. According to the flow geometry, we suggest the boundary conditions

$$u = 0, \text{ at } r = r_2, \tag{7}$$

$$u = V, \text{ at } r = r_1, \tag{8}$$

where V implies the inner cylinder velocity. The dimensionless quantities used in the current investigation can be stated as

$$r' = \frac{r}{a},\ z' = \frac{z}{\lambda},\ u' = \frac{u}{c},\ v' = \frac{\lambda}{ac}v,\ t = \frac{c}{\lambda}t,$$
$$\phi = \frac{b}{a},\ \delta' = \frac{\delta}{a},\ \varepsilon' = \frac{\varepsilon}{a},\ \delta_0 = \frac{a}{\lambda},$$
$$p' = \frac{a^2}{\mu c \lambda}p,\ \mathrm{Re} = \frac{\rho c a}{\mu},\ M'^2 = \frac{\sigma B_0^2 a^2}{\mu},\ \theta' = \theta,$$
$$V' = \frac{V}{c},\ k' = \frac{k_1}{a^2},\ \psi' = \frac{\psi}{ca},\ S' = \frac{a}{\mu c}S, \tag{9}$$

where ϕ is the amplitude ratio, t is the time parameter, Re

is the Reynold's number, δ_0 is the wave number, M provides the MHD contribution parameter, and k is the porosity parameter. After taking into account the above parameters, the corresponding flow equations are incorporated into the consequential form

$$\mathrm{Re}\,\delta_0^3\left[\frac{\partial v}{\partial t}+\frac{\partial v}{\partial z}+\frac{\partial v}{\partial r}\right]=-\frac{\partial p}{\partial r}+\frac{\delta_0}{r}\frac{\partial}{\partial r}(rS_{rr})+\frac{\delta_0}{r}\frac{\partial}{\partial\theta}(S_{r\theta})+\delta_0^2\frac{\partial}{\partial z}(S_{rz})-\delta_0\frac{S_{\theta\theta}}{r}-\delta_0^2M^2v-\delta_0^2\frac{v}{k}, \tag{10}$$

$$0=-\frac{1}{r}\frac{\partial p}{\partial\theta}+\frac{\delta_0}{r^2}\frac{\partial}{\partial r}(r^2S_{r\theta})+\frac{\delta_0}{r}\frac{\partial}{\partial\theta}(S_{\theta\theta})+\delta_0^2\frac{\partial}{\partial z}(S_{\theta z}), \tag{11}$$

$$\mathrm{Re}\,\delta_0\left[\frac{\partial u}{\partial t}+u\frac{\partial u}{\partial z}\right]=-\frac{\partial p}{\partial z}+\frac{1}{r}\frac{\partial}{\partial r}(rS_{rz})+\frac{1}{r}\frac{\partial}{\partial\theta}(S_{\theta z})+\delta_0\frac{\partial}{\partial z}(S_{zz})-M^2u-\frac{u}{k}. \tag{12}$$

The dimensionless components of stress are expanded as

$$\begin{aligned}
S_{rr}&=\frac{2\delta_0}{1+\lambda_1}\left(1+\frac{\lambda_2c\delta_0}{a}\left(\frac{\partial}{\partial t}+v\frac{\partial}{\partial r}+u\frac{\partial}{\partial z}\right)\right)\frac{\partial v}{\partial r},\\
S_{r\theta}&=\frac{\delta_0}{1+\lambda_1}\left(1+\frac{\lambda_2c\delta_0}{a}\left(\frac{\partial}{\partial t}+v\frac{\partial}{\partial r}+u\frac{\partial}{\partial z}\right)\right)\frac{1}{r}\frac{\partial v}{\partial\theta},\\
S_{rz}&=\frac{1}{1+\lambda_1}\left(1+\frac{\lambda_2c\delta_0}{a}\left(\frac{\partial}{\partial t}+v\frac{\partial}{\partial r}+u\frac{\partial}{\partial z}\right)\right)\left(\delta_0^2\frac{\partial v}{\partial z}+\frac{\partial u}{\partial r}\right),\\
S_{\theta\theta}&=\frac{2\delta_0}{1+\lambda_1}\left(1+\frac{\lambda_2c\delta_0}{a}\left(\frac{\partial}{\partial t}+v\frac{\partial}{\partial r}+u\frac{\partial}{\partial z}\right)\right)\frac{v}{r},\\
S_{\theta z}&=\frac{1}{1+\lambda_1}\left(1+\frac{\lambda_2c\delta_0}{a}\left(\frac{\partial}{\partial t}+v\frac{\partial}{\partial r}+u\frac{\partial}{\partial z}\right)\right)\frac{1}{r}\frac{\partial u}{\partial\theta},\\
S_{zz}&=\frac{2\delta_0}{1+\lambda_1}\left(1+\frac{\lambda_2c\delta_0}{a}\left(\frac{\partial}{\partial t}+v\frac{\partial}{\partial r}+u\frac{\partial}{\partial z}\right)\right)\frac{\partial u}{\partial z}.
\end{aligned} \tag{13}$$

Using the constraints of long wavelength and less Reynolds number, the observing equations (10-12) approach the following form:

$$\frac{\partial p}{\partial r}=0, \tag{14}$$

$$\frac{\partial p}{\partial\theta}=0, \tag{15}$$

$$(1+\lambda_1)\frac{\partial p}{\partial z}=\frac{\partial^2u}{\partial r^2}+\frac{1}{r}\frac{\partial u}{\partial r}+\frac{1}{r^2}\frac{\partial^2u}{\partial\theta^2}-\frac{(1+\lambda_1)}{r^2}M^2u-\frac{(1+\lambda_1)}{r^2}\frac{u}{k}$$

$$(1+\lambda_1)\frac{\partial p}{\partial z}=\frac{\partial^2u}{\partial r^2}+\frac{1}{r}\frac{\partial u}{\partial r}+\frac{1}{r^2}\frac{\partial^2u}{\partial\theta^2}-\frac{\xi^2}{r^2}u. \tag{16}$$

In the above expression, we have $\xi=\sqrt{(1+\lambda_1)(M^2+1/k)}$

Eqs. (14) and (15) suggest that p is independent of r and θ. The non-dimensional boundary conditions attain the form

$$u=0,\quad \text{at } r=r_2=1+\varphi\cos\left[2\pi(z-t)\right], \tag{17}$$

$$u=V,\quad \text{at } r=r_1=\delta+\varepsilon\cos\theta. \tag{18}$$

3. Solution to the Problem

The solution to Eq. (16) is acquired by using the well-known perturbation method [15-16]. The deformation equation for the present problem is suggested as

$$H(u,q)=(1-q)\left(L[\hat{u}]-L[\hat{u}_0]\right)+q\left(L[\hat{u}]+\frac{1}{r^2}\frac{\partial^2\hat{u}}{\partial\theta^2}-(1+\lambda_1)\frac{dp}{dz}\right)=0, \tag{19}$$

where q is the embedding parameter, and the linear operator is chosen to be $L=\frac{\partial^2}{\partial r^2}+\frac{1}{r}\frac{\partial}{\partial r}-\frac{\xi^2}{r^2}$. We consider the subsequent initial guess

$$\hat{u}_0=V\frac{\sinh\left(\xi(\log[r]-\log[r_2])\right)}{\sinh\left(\xi(\log[r_1]-\log[r_2])\right)}. \tag{20}$$

Now we suggest

$$\hat{u}_0(r,\theta,z,t,q)=u_0+qu_1+\ldots \tag{21}$$

Applying the above series to Eq. (19) and equating the terms of the successive powers of q, we achieve the following systems:

$$L[u_0]-L[\hat{u}_0]=0, \tag{22}$$

$$u_0=0,\quad \text{at } r=r_2,\ u_0=V,\quad \text{at } r=r_1, \tag{23}$$

$$\frac{\partial^2u_1}{\partial r^2}+\frac{1}{r}\frac{\partial u_1}{\partial r}-\frac{\xi^2}{r^2}u_1-(1+\lambda_1)\frac{dp}{dz}+\frac{1}{r^2}\frac{\partial^2u_0}{\partial\theta^2}=0, \tag{24}$$

$$u_1=0,\quad \text{at } r=r_2,\ u_1=0,\quad \text{at } r=r_1. \tag{25}$$

Eqs. (20) and (22) provide the solution of the zeroth-order system, and is described in the relation

$$u_0(r,\theta,z,t,q)=\hat{u}_0=V\frac{\sinh\left(\xi(\log[r]-\log[r_2])\right)}{\sinh\left(\xi(\log[r_1]-\log[r_2])\right)}. \tag{26}$$

The solution of the first order system is summarized as

$$u_1=\frac{1}{4\sqrt{(1+\lambda_1)(M^2+1/k)}\left(\sqrt{(1+\lambda_1)(M^2+1/k)}^2-4\right)}$$

$$(A_1)\left(\left(-4\sqrt{(1+\lambda_1)(M^2+1/k)}\frac{dp}{dz}r_2^2+A_5\left((1+\lambda_1)(M^2+1/k)-4\right)\log\left[\frac{rr_1}{r_2^2}\right]\right)$$

$$\times A_2 - A_5\left((1+\lambda_1)(M^2+1/k)-4\right)\log\left[\frac{r}{r_1}\right]A_3\Big) \quad (27)$$
$$+4\sqrt{(1+\lambda_1)(M^2+1/k)}\,\frac{dp}{dz}\left(r_1^2\times A_4 - r^2/A_1\right.$$
$$\left.-4\sqrt{(1+\lambda_1)(M^2+1/k)}\,\frac{dp}{dz}\left(r_2^2A_2 - r_1^2A_4 + \right)r^2/A_1\right)\lambda_1\Big)\Big),$$

where

$$A_1 = \operatorname{csch}\left(\sqrt{(1+\lambda_1)(M^2+1/k)}\log\left[\frac{r_1}{r_2}\right]\right),$$
$$A_2 = \sinh\left(\sqrt{(1+\lambda_1)(M^2+1/k)}\log\left[\frac{r}{r_1}\right]\right),$$
$$A_3 = \sinh\left(\sqrt{(1+\lambda_1)(M^2+1/k)}\log\left[\frac{rr_1}{r_2^2}\right]\right),$$
$$A_4 = \sinh\left(\sqrt{(1+\lambda_1)(M^2+1/k)}\log\left[\frac{r}{r_2}\right]\right),$$
$$A_5 = \frac{1}{r_1^2}\left(\xi V\varepsilon\operatorname{csch}\left(\xi\log\left[\frac{r_1}{r_2}\right]\right)\left((\varepsilon+\delta\cos\theta)\coth\left(\xi\left(\log\left[\frac{r_1}{r_2}\right]\right)\right)\right.\right.$$
$$\left.\left.+\xi\varepsilon\left(1+2\operatorname{csch}^2\left(\xi\left(\log\left[\frac{r_1}{r_2}\right]\right)\right)\right)\sin^2\theta\right)\right).$$

Now for $q \to 1$, we set the required solution. So Eq. (21) implies

$$u(r,\theta,z,t) = u_0 + u_1 + ...$$

where u_0 and u_1 are evaluated in Eqs. (26) and (27). The momentary volume flow rate $\overline{Q}(z,t)$ is written as

$$\overline{Q}(z,t) = 2\pi\int_{r_1}^{r_2} rudr, \quad (28)$$

$$\overline{Q}/2\pi = \frac{1}{4\xi(\xi^2-4)^2}\left((\xi^2+4)\left(2A_5r_2^2+\xi\frac{dp}{dz}(r_1^4-r_2^4)\right)\right.$$
$$+8\xi(\xi^2-4)r_1^2V - 2A_5(\xi^2+4)r_1^2\times\Big)$$
$$\cosh\left(\xi\log\left[\frac{r_1}{r_2}\right]\right) + 2\xi\operatorname{csch}\left(\xi\log\left[\frac{r_1}{r_2}\right]\right)$$
$$\left(2\xi r_2^2\left(2\frac{dp}{dz}r_1^2+(\xi^2-4)V\right) - A_5(\xi^2-4)r_1^2\times\right)$$
$$\log\left[\frac{r_1}{r_2}\right]\Big) - 2\xi\coth\left(\xi\log\left[\frac{r_1}{r_2}\right]\right) \quad (29)$$
$$\left(2\xi\left(\frac{dp}{dz}(r_1^4+r_2^4)+(\xi^2-4)r_1^2V\right) - A_5(\xi^2-4)r_2^2\times\right)$$
$$\log\left[\frac{r_1}{r_2}\right]\Big) + 8A_5\xi r_1^2\sinh\left(\xi\log\frac{r_1}{r_2}\right) + \xi\frac{dp}{dz}\left((\xi^2+4)(r_1^4-r_2^4)\right.$$
$$\left.-4\xi(r_1^4+r_2^4)\coth\left(\xi\log\frac{r_1}{r_2}\right)+\right)8\xi r_1^2r_2^2\operatorname{csch}\left(\xi\log\frac{r_1}{r_2}\right)\Big)\lambda_1\Big)\Big).$$

Now $\overline{Q}$, the mean volume flow rate measured for one period is given as [12]

$$\overline{Q}(z,t) = \frac{Q}{\pi} - \frac{\varphi^2}{2} + 2\varphi\cos[2\pi(z-t)] + \varphi^2\cos^2[2\pi(z-t)], \quad (30)$$

where Q accounts for the average flow per period of the wave. Now we can execute the expression of pressure gradient dp/dz by incorporating Eqs. (29) and (30) and extracting it as

$$\frac{dp}{dz} = \left(2\left(-4A_5\pi r_2^2 + \xi\left(2(\xi^2-4)^2Q + \pi\left(A_5\xi r_2^2 - 4(\xi^2-4)r_1^2V\right)\right)\right.\right.$$
$$+\xi(\xi^2-4)^2\pi\varphi\times\Big)\left(4\cos[2\pi(z-t)]+\varphi\cos[4\pi(z-t)]\right)$$
$$+A_5(\xi^2+4)\pi r_1^2\cosh\left(\xi\log\left[\frac{r_1}{r_2}\right]\right)+\xi\pi\Big)\operatorname{csch}\left(\xi\log\frac{r_1}{r_2}\right)$$
$$\left(2A_5r_1^2 - 2\xi(\xi^2-4)r_2^2V + A_5r_1^2\left(2\cosh\left(2\xi\log\frac{r_2}{r_1}\right)+(\xi^2-4)\log\frac{r_1}{r_2}\right)\right)$$
$$\left.\left.+(\xi^2-4)\cosh\left(\xi\log\left[\frac{r_1}{r_2}\right]\right)\left(2\xi r_1^2V + A_5r_2^2\log\left[\frac{r_2}{r_1}\right]\right)\right)\right)\right)$$
$$/\left(\xi\pi\left((\xi^2+4)(r_1^4-r_2^4)\right)\right.$$
$$-4\xi(r_1^4-r_2^4)\coth\left(\xi\log\left[\frac{r_1}{r_2}\right]\right)+\Big)$$
$$\left.8\xi r_1^2r_2^2\operatorname{csch}\left(\xi\log\left[\frac{r_1}{r_2}\right]\right)(1+\lambda_1)\Big)\right). \quad (31)$$

The non-dimensional form of pressure rise is calculated as

$$\Delta p(t) = \int_0^1 \frac{\partial p(z,t)}{\partial z}dz. \quad (32)$$

4. Outcomes and Explanations

The series and numerical data evaluated above are discussed in this section with reference to figures and tables. The present results are also compared with those already acquired by Ellahi *et al*. [14]. The graphical consequences for the data of pumping profile Δp, pressure gradient dp/dz and velocity component $u(r, \theta, z, t)$ are executed with the alternate values of porosity parameter k and the magnetic field parameter M. The stream lines displaying the imaginary flow behavior are sketched for M and k.

Table 1 has been compiled to clarify the comparison of the present results with the literature. The comparison of this study with that of Ellahi *et al.* [14] is also disclosed in Fig. 2. The graph for $\Delta p(t)$ against the flow rate Q under the variation of the considered parameters is visualized in Fig. 3. This graph explains the variation of pressure rise in the pumping parts, which is to say, the peristaltic pumping ($Q > 0$, $\Delta p > 0$) the augmented pumping

Table 1. Comparison of present velocity data with that obtained by Ellahi *et al.* [14].

	Ellahi *et al.* [14] for	Present work for	Present work for
r	V=0.1	$k\to\infty$, V=0.1	K=0.1, V=0.1
0.30	0.10000	0.10000	0.00000
0.4	0.63386	0.63386	0.43656
0.5	0.95027	0.95027	0.68894
0.6	1.10889	1.10889	0.90114
0.7	1.13215	1.13215	1.04966
0.8	1.02961	1.02961	1.09172
0.9	0.80562	0.80562	0.97374
1.0	0.46215	0.46215	0.63338
1.1	0.00000	0.00000	0.00000

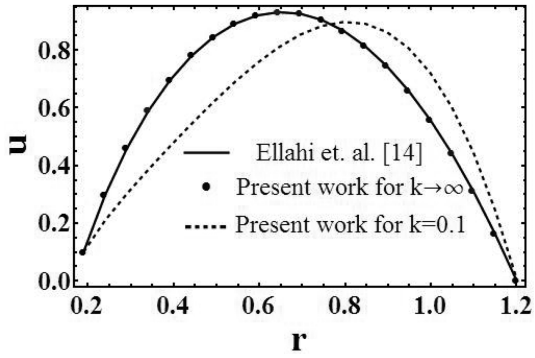

Fig. 2. Comparison of present velocity distribution with Ellahi *et al*. [14] for fixed $\delta = 0.1$, $\theta = 0.8$, $\phi = 0.1$, $z = 0$, $t = 0.2$, $M = 1$, $\varepsilon = 0.1$, $Q = 0.7$, $\lambda_1 = 0.5$.

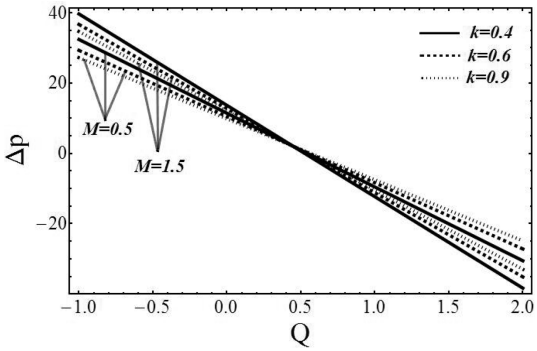

Fig. 3. Pressure rise Δp for k and M. The other parameters are $\varepsilon = 0.1$, $\phi = 0.2$, $t = 0.2$, $\delta = 0.2$, $\lambda_1 = 0.5$, $V = 0.1$, $\theta = 0.8$.

($Q > 0$, $\Delta p < 0$), and the reverse pumping ($Q < 0$, $\Delta p > 0$) The pressure gradient dp/dz with the variation of the relevant parameters is drawn in Fig. 4. The axial velocity component $u(r, \theta, z, t)$ is plotted in Fig. 5 for various pertinent quantities. The stream line graphs are shown in Figs. 6 and 7.

It is obvious from Table 1 and Fig. 2 that the results measured in the present analysis are consistent with those

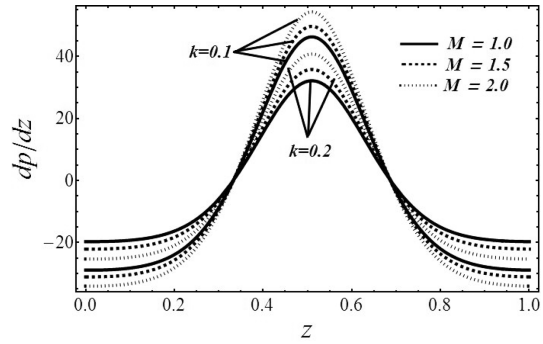

Fig. 4. Pressure gradient dp/dz for k and M. The other parameters are $\delta = 0.1$, $\phi = 0.2$, $t = 0.01$, $\varepsilon = 0.1$, $Q = 0.6$, $V = 0.1$, $\lambda_1 = 0.5$, $\theta = 0.8$.

of the study by Ellahi *et al.* [14] throughout the flow. It is also confirmed that the contribution of the porous medium for non-Newtonian Jeffrey fluid results in the reduction of the velocity in region $r \in (0.2, 0.8)$ but makes the flow faster in the remaining part. It is clear from Fig. 3 that the peristaltic pumping region encloses the interval $Q \in [0, 0.8)$, the augmented pumping $Q \in [0.8, 2]$, and the retrograde pumping part $Q \in [-1, 0)$. The variation of pressure rise Δp for porosity parameter k and MHD parameter M is examined in Fig. 3, and it is apparent from this graph that there is an appendage in pressure rise with varying M but a decline with the parameter k in the peristaltic as well as retrograde pumping, and quite the opposite analysis is measured on the augmented side. It can be suggested from Fig. 4 that the pressure gradient increases in the interim area of the domain but lessens in the broader parts with the increase in the values of the MHD parameters M while the reverse attitude is calculated for the porosity parameter k. So, it can be declared that in the presence of a porous medium, a large amount of pressure will conserve the flow rate in the middle of the flow stream rather than the side walls, which is also obvious physically. It is also shown in this graph that the pressure gradient gets its depth on the left and right channels of the cylinder while the peak is approached at the centre. This implies, significantly, that fluid can travel without imposing extra pressure in the two sides of the channel, while in the central part close to $z = 0.5$, a large pressure gradient is necessary in order to stabilize the flow rate. This is in good agreement with the experimental evidence. It is learned from Fig. 5 that the velocity component increases with k in $0.2 < r < 0.7$ region whereas it diminishes on the $0.7 \le r \le 1.1$ side, meanwhile, the totally reverse conclusion is extracted for the MHD parameter M. Figure 6 displays the pattern of stream lines along the magnetic field parameter M. From

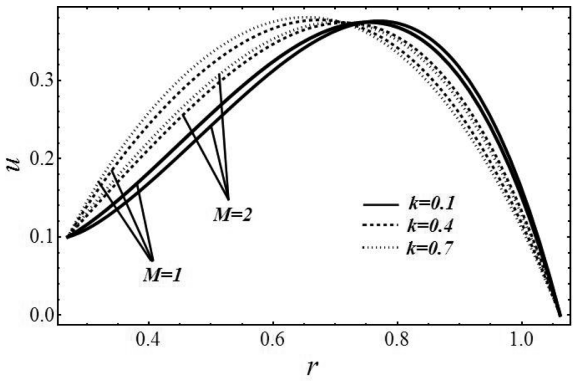

Fig. 5. Profile of axial velocity u for k and M. The other parameters are $\delta = 0.2$, $\phi = 0.2$, $t = 0.2$, $z = 0$ $\varepsilon = 0.1$, $Q = 0.1$, $V = 0.1$, $\lambda_1 = 0.5$, $\theta = 0.8$.

this figure, it is determined that there is an increase in the number of boluses and that the size changes manually in the upper half of the domain while the quantity of boluses remains fixed but the size increases with the increasing effects of M in the bottom of the flow. Fig. 7 indicates that the numbers of boluses decrease with different values of parameter k in upper region but remain consistent in the lower region while the size expands on both sides of the flow range.

5. Concluding Remarks

In this paper, the authors have presented the peristaltic flow of Jeffrey fluid in the presence of a magnetic field and a porous medium. The governing equations are modeled under the consideration of some physical limitations. The analytical and numerical results are found and are discussed in graphs. The main findings of the above analysis are made on the basis of graphical results and can be summarized as follows:

1. The results achieved in this work are consistent with those of a previous study [14] throughout the flow for very large values of permeability factor k.

2. The inclusion of a porous medium result in the reduction of the velocity in the left region of the body but increases in the remaining parts though the magnetic field

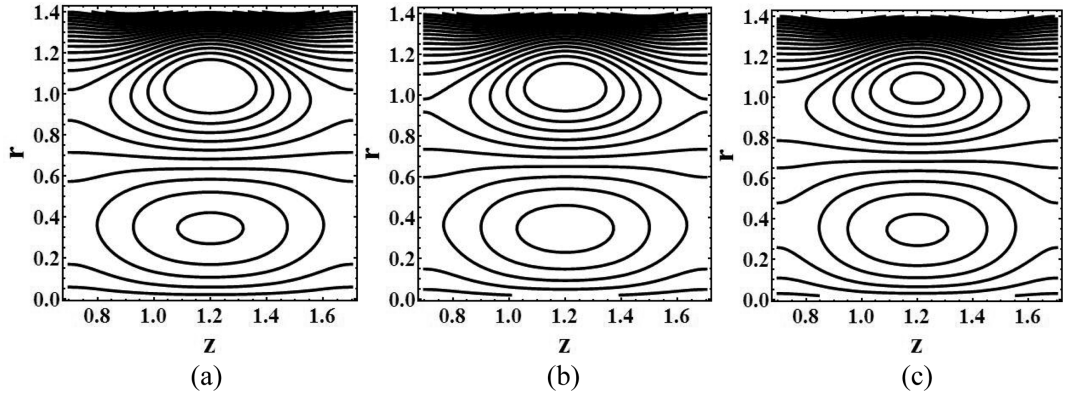

Fig. 6. Stream lines against M. (a) for $M = 0.1$, (b) for $M = 0.3$, (c) for $M = 0.5$. The fixed quantities are $\varepsilon = 0.4$, $V = 0.1$, $t = 0.2$, $\theta = 0.8$, $\phi = 0.05$, $k = 0.9$, $Q = 0.6$, $\delta = 0.05$, $\lambda_1 = 0.5$.

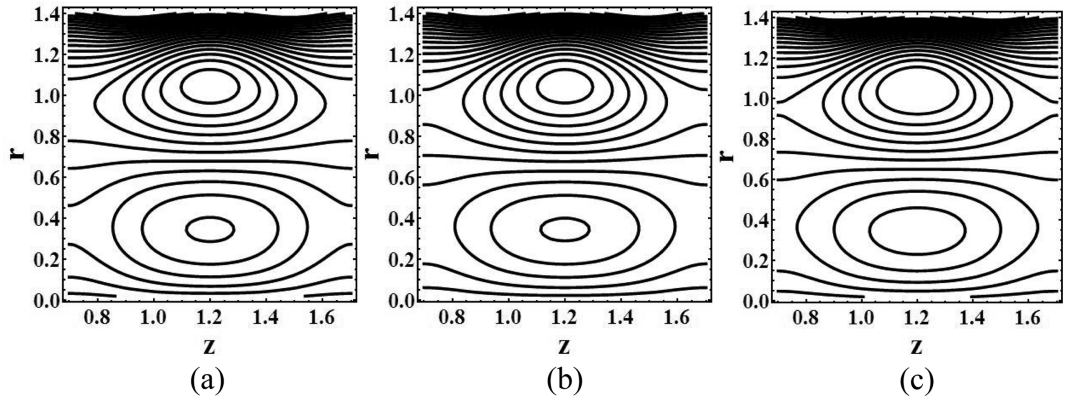

Fig. 7. Stream lines against k. (a) for $k = 0.8$, (b) for $k = 0.9$, (c) for $k = 1$. The fixed quantities are $\varepsilon = 0.4$, $V = 0.1$, $t = 0.2$, $\theta = 0.8$, $\phi = 0.05$, $Q = 0.6$, $M = 0.3$, $\delta = 0.05$,$\lambda_1 = 0.5$.

suggests that the outcomes are contrary to the magnetic field.

3. The presence of a magnetic field increases the peristaltic pumping rate but the porous medium decreases it.

4. The pressure gradient increases in the central part but decreases at the corners with the increase in the MHD parameters, whereas the permeability of the medium reveals the opposite behavior.

References

[1] S. Srinivas and M. Kothandapani, Appl. Math. Comput. **213**, 197 (2009).
[2] M. M. Bhatti, R. Ellahi, and A. Zeeshan, J. Mol. Liq. **222**, 101 (2016).
[3] M. M. Bhatti, A, Zeeshan, R. Ellahi, and N. Ijaz, J. Mol. Liq. **230**, 237 (2017).
[4] R. Ellahi, E. Shivanian, S. Abbasbandy, and T. Hayat, Int. J. Numer. Meth. Heat Fluid Flow **26**, 1433 (2015).
[5] M. M. Bhatti, A, Zeeshan, and R. Ellahi, Microvasc. Res. **110**, 32 (2017).
[6] A. Khan, H. Usman, K. Vafai, and R. Ellahi, Sci. Iran. **23**, 2650 (2016).
[7] M. M. Bhatti, A, Zeeshan, and R. Ellahi, Comput. Biol. Med. **78**, 29 (2016).
[8] M. V. S. Reddy, M. Mishra, S. Sreenadh, and A. R. Rao, J. Fluids Eng. **127**, 824 (2005).
[9] J. M. Nouri, H. Umur, and J. H. Whitelaw, J. Fluid Mech. **253**, 617 (1993).
[10] I. C. Walton and S. H. Bittlestone, J. Fluid Mech. **222**, 39 (1991).
[11] S. Nadeem, A. Riaz, R. Ellahi, and N. S. Akbar, Appl. Nanosci. **4**, 393 (2014).
[12] K. S. Mekheimer, Y. Abdelmaboud, and A. I. Abdellateef, Appl. Bionics. Biomech. **10**, 19 (2013).
[13] K. S. Mekheimer, Y. Abdelmaboud, and A. I. Abdellateef, Int. J. BioMath. **6**, 25 (2013).
[14] R. Ellahi, A. Riaz, S. Nadeem, and M. Mushtaq, Appl. Math. Inf. Sci. **7**, 1441 (2013).
[15] J. H. He, Phys. Lett. A. **350**, 87 (2006).
[16] J. H. He, Comp. Meth. Appl. Mech. Eng. **178**, 257 (1999).